

# Segmenting Individual Trees From Terrestrial LiDAR Data Using Tree Branch Directivity

Zekun Yang , Yanjun Su , Wenkai Li , Kai Cheng , Hongcan Guan , Yu Ren , Tianyu Hu ,  
Guangcai Xu , and Qinghua Guo 

**Abstract**—Over the last decade, a number of techniques for individual tree segmentation has been developed for terrestrial laser scanning data. The superpoint segmentation algorithm based on point cloud has been widely used in individual tree segmentation because of its high efficiency and numerous geometric features. However, this algorithm is generally developed for specific tree species and forest types, limiting its universality and performance for different forest types. To handle this problem, a new method based on the topology of tree branches for individual tree segmentation was proposed. Focusing on the general topological structure of trees, the proposed method iteratively assigns each branch based on its directivity to its upper branch at the superpoint level. The proposed method was tested compared with the original superpoint method and an ecological method in six sample plots with different forest conditions. In such plots, the proposed method achieved anticipated performance with an average accuracy of 40% improvements compared with the other two methods, especially in complicated forest conditions. Experimental results also showed an improved average accuracy of 70% compared with the original superpoint method at the point level. This proposed method can effectively expand the universality of the superpoint method to further advance ecological and forest research.

**Index Terms**—Directivity, individual tree segmentation, point cloud, superpoint, terrestrial laser scanning (TLS).

## I. INTRODUCTION

**F**OREST inventory is an indispensable part in the process of managing forest resources. An essential part of forest

Manuscript received 21 June 2023; revised 21 September 2023; accepted 6 November 2023. Date of publication 17 November 2023; date of current version 6 December 2023. This work was supported in part by the National Key Research and Development Program under Grant 2022YFF1300203, in part by the International Research Center of Big Data for Sustainable Development Goals under Grant CBAS2022GSP06, and in part by the National Natural Science Foundation of China under Grant 31971575. (Corresponding author: Qinghua Guo.)

Zekun Yang, Kai Cheng, Yu Ren, and Qinghua Guo are with the Institute of RS and GIS, School of Earth and Space Sciences, Peking University, Beijing 100871, China (e-mail: nebel@pku.edu.cn; kai\_cheng@pku.edu.cn; renyu\_rs@pku.edu.cn; guo.qinghua@pku.edu.cn).

Yanjun Su and Tianyu Hu are with the State Key Laboratory of Vegetation and Environmental Change, Institute of Botany, Chinese Academy of Sciences, Beijing 100093, China, and also with the University of Chinese Academy of Sciences, Beijing 100049, China (e-mail: ysu@ibcas.ac.cn; tianyuhu@ibcas.ac.cn).

Wenkai Li is with the School of Geography and Planning, Sun Yat-Sen University, Guangzhou 510006, China (e-mail: liwenk3@mail.sysu.edu.cn).

Hongcan Guan is with the School of Tropical Agriculture and Forestry, Hainan University, Haikou 570100, China (e-mail: guanhongcan@gmail.com).

Guangcai Xu is with the Beijing GreenValley Technology Company, Ltd., Beijing 100091, China (e-mail: xugc@lidar360.com).

This article has supplementary downloadable material available at <https://doi.org/10.1109/JSTARS.2023.3334014>, provided by the authors.

Digital Object Identifier 10.1109/JSTARS.2023.3334014

inventory is the acquisition of forest structure characteristics [1]. Depending on the scale, forest structure characteristics can be divided into plot scale and individual tree scale [2], [3]. Traditionally, forest structure characteristics are obtained by means of in situ observations [4], [5], [6]. However, due to the wide distribution of forest resources, it is generally cost-prohibitive to conduct in situ observations of forest structure at fine spatial scales across large areas [7], [8].

In the past two decades, light detection and ranging (LiDAR) has become a major technique for forest structure research, offering a cost-effective solution [9], [10]. As an active remote sensing technology, LiDAR can depict the internal structure of vegetation canopies and has the potential to overcome the challenges of in situ observations [11], [12]. Among various LiDAR platforms, terrestrial laser scanning (TLS) can obtain high-precision point clouds with high-quality and high-density data for quantitative research on forest structure [13], [14], [15]. However, because of the complexity of forest structure and the disorderly nature of laser point clouds, individual tree segmentation of forest point clouds is necessary for obtaining individual tree scale characteristics [16], [17], [18], [19]. Thus, individual tree segmentation based on TLS data has been widely studied [20], [21].

At present, there are two main categories of individual tree segmentation algorithms based on LiDAR data [22]. The first method uses the canopy height model (CHM) for individual tree segmentation. CHM is a model that reflects the vertical height of the forest canopy surface from the ground, directly providing the horizontal and vertical distribution of the canopy. This method mainly maps the 3-D forest point cloud into a 2-D raster, which is then analyzed with image processing or computer vision techniques to extract the horizontal and vertical features of the canopy needed to segment individual trees. This method has been widely used for its simplicity and high efficiency in data processing [22], [23]. Watershed segmentation, moving window maximum, multiscale segmentation method, and some deep-learning methods can all be classified into this category [24], [25]. For example, Amiri [26] segmented individual trees using a marker watershed segmentation method by detecting treetops on various scale. Hu et al. [24] proposed a marked watershed segmentation algorithm, which realized the segmentation of Canadian deciduous and mixed forests with an accuracy greater than 70%. However, this method is not suitable for closely overlapping trees and multilayer coniferous forests and may introduce additional errors in the process of transforming a 3-D point cloud

into a 2-D grid. Besides, some forest 3-D structure information can be lost, resulting in low-accuracy segmentation [22].

The second method is fully based on point cloud data, and some classical algorithms, such as clustering algorithm and voxel segmentation algorithm, can be classified into this category. These algorithms utilize computer vision technology and combine knowledge of trees' morphology and ecology, such as point density, normal vector, 3-D spatial distribution, and other features, for individual tree segmentation [27], [28], [29]. This method can better make use of the rich 3-D structure information in point cloud data, achieving good segmentation accuracy in complicated forest conditions where trees are closely overlapped. For example, Tao et al. [30] constructed a comparative path shortest algorithm to segment the crowns based on the theory of metabolic ecology and the fact that vascular plants tend to minimize the transport distance to the root. Good segmentation results have been observed in both coniferous and broad-leaved forests. Huo et al. [25] took advantage of the symmetrical structure of trees and constructed an algorithm for identifying the underlying vegetation of forests. Results with more than 90% accuracy were obtained in the segmentation of three kinds of woodlands. At present, the hypervoxel-based segmentation algorithm has also been widely studied in the field of individual tree segmentation because of its high efficiency. Hypervoxel is an aggregation of a series of voxels that carries more semantic information about point clouds. This kind of algorithm combines the characteristics of object segmentation and completes the steps of individual tree segmentation efficiently and accurately [28]. For example, Wang [29] constructed an unsupervised individual tree segmentation algorithm based on the hypervoxel using the morphological characteristics of trees, obtaining accurate results on simulation data.

However, these hypervoxel-based (superpoint-based) methods are usually suitable for certain trees because in the tree segmentation process, tree topology is constructed according to the geometric properties of hypervoxels but neglecting the way how tree topology formed. Different construction method of hypervoxels tend to only suitable for specific tree species and forest types, lacking universality. From the point of view of tree morphology, the natural positivity and geotropy of trees indicate the orientation of the branches is certain. Considering all branches are geometrically close to the upper branch, the skeleton can be easily constructed by merging branches according to certain directivity when making use of the directional growth of branches with respect to the trunk. To our best knowledge, this proposed method is the first method to combine hypervoxel with the branch directivity and a practical way to expand the applicability of the superpoint algorithm to various forest types. To validate the proposed method, six sample plots of typical forest types were selected, including temperate artificial broad-leaved forest, temperate artificial coniferous forest, temperate natural broadleaf and mixed forests, temperate natural broad-leaved forest, subtropical broad-leaved forest, and tropical rain forest. To demonstrate its effectiveness, the proposed method was compared to the original unsupervised hypervoxel segmentation method developed by Wang [29] and an ecological segmentation method using LiDAR360 software [30].

## II. DATA

### A. Study Area

To further evaluate the universality, six sample plots of different forest types were selected to validate the algorithm, which can represent forests of different complexities. Among them, five sample plots are collected from China, which can represent typical forest types in China. Their types vary from planted broad-leaved forest, planted coniferous forest, natural mixed conifer broad-leaved forests, subtropical broad-leaved forest, tropical rain forest, and natural broad-leaved forest. The data in plot 1 were downloaded from the publicly available dataset released by SimpleForest (<https://simpleforest.org/pages/dataTest.html>), while the other data in plots 2, 3, 4, 5, and 6 were collected in various forest regions of China (Table I). Plots 1 and 2 were both plantations of 10 m × 10 m, with stand densities of 1596 and 1980 plants/ha, respectively (Table I). The average tree heights were 14.7 and 8.8 m, respectively. Plot 1 was a natural broad-leaved forest in northeastern France scanned by the Faro scanner, and the dominant tree species were *Quercus* and *Fagus* and the laser point density was 3528 pts/m<sup>2</sup>. Plot 2 was a planted coniferous forest located in Mulan Paddock, Hebei Province, China, dominated by *Prince Rupprecht's larch* and *Pinus tabulaeformis*. The LiDAR data were acquired by a Rigel VZ-400 with a point density of 3970 pts/m<sup>2</sup>. The Rigel VZ-400 was also used for the acquisition of TLS data in the remaining plots (plots 3, 4, 5, and 6). Plot 3 was a mixed conifer broad-leaved forests located in Qinling mountains, Shaanxi Province, Central China, dominated by *Quercus glauca*, *Pinus massoniana*, and *Lindera reflexa Hemsl.* Plot 4 was a subtropical broad-leaved forest located in Dinghushan Nature Reserve, Guangdong Province, Southern China, with a plot size of 25 m × 25 m. The average tree height was about 14.7 m, and the dominant tree species were *Castanopsis chinensis*, *Schima superba* (Table I). Plot 5 was a tropical rain forest located in Jianfengling National Forest Park, Hainan Province, China, with an area of 30 m × 30 m and dominated by *Litchi chinensis*, *Xanthophyllum hainanense*, *Dacrycarpus imbricatus*. Plot 6 was a natural broad-leaved forest, located in Changbai Mountain, Jilin Province, China, with an area of 30 m × 30 m and dominated by *Pinus koraiensis*, *Tilia*, *Quercus mongolica* (Table I). Plots 4, 5, and 6 had the most complicated forest conditions, including tall arbors and a lot of thickets under the forests (Fig. 1).

### B. Preprocessing

Point clouds in plot 1 were downloaded from open dataset and were preprocessed before. After collecting the TLS point cloud using Rigel VZ-400, plots 2, 3, 4, 5, and 6 were stitched and registered (Table II). Each plot had 24 high-reflectivity targets placed to make sure that at least four targets were scanned each time, with a total of six scans completed per plot. Afterward, the TLS point cloud on each plot was registered using a marker-free multistation TLS point cloud registration method [20]. Then, outlier removal, ground point filtering, and normalization were performed on the registered data by LiDAR360 software (Green Valley International). Outlier removal mainly removed noise

TABLE I  
BASIC INFORMATION ABOUT SIX SCANNED FOREST PLOTS

Plot	Location	Size(m <sup>2</sup> )	Forest type	Stand density	Highest tree height (m)	Average tree height (m)	Dominant species	Scan device
1	Northeast France	10 × 10	Planted broad-leaved forest	1596 plants/ha	20.2	16.6	<i>Quercus, Fagus</i>	Faro Photon 120™
2	Mulan paddock	10 × 10	Planted coniferous forest	1980 plants/ha	11.4	8.8	<i>Larix principis-rupprechtii</i> Mayr, <i>Pinus tabulaeformis</i>	Rigel VZ-400
3	Qinling Mountains	20 × 20	Natural mixed conifer broad-leaved forests	2850 plants/ha	20.6	8.2	<i>Quercus glauca, Pinus massoniana, Lindera reflexa</i> Hemsl	Rigel VZ-400
4	Dinghu Mountain	25 × 25	Natural subtropical broad-leaved forest	1129 plants/ha	29.0	14.7	<i>Castanopsis chinensis, Schima superba</i>	Rigel VZ-400
5	Jianfengling National Forest Park	30 × 30	Tropical rain forest	1211 plants/ha	29.9	9.4	<i>Litchi chinensis, Xanthophyllum hainanense, Dacrycarpus imbricatus</i>	Rigel VZ-400
6	Changbai Mountain	30 × 30	Natural broad-leaved forest	1023 plants/ha	27.3	18.1	<i>Pinus koraiensis, Tilia, Quercus mongolica</i>	Rigel VZ-400

TABLE II  
SPECIFICATION OF FARO PHOTON 120™ AND RIGEL VZ-400 TERRESTRIAL LIDAR SYSTEM

Scanning parameters	Field of view	Scanning range	Scanning accuracy	Effective measurement rate
<b>Faro Photon 120™</b>	Horizontal: 360° Vertical: 320°	503 m	2 mm at 10 m distance	976 000 pts/s
<b>Rigel VZ-400</b>	Horizontal: 360° Vertical: 100°	600 m	2 mm at 100 m distance	122 000 pts/s

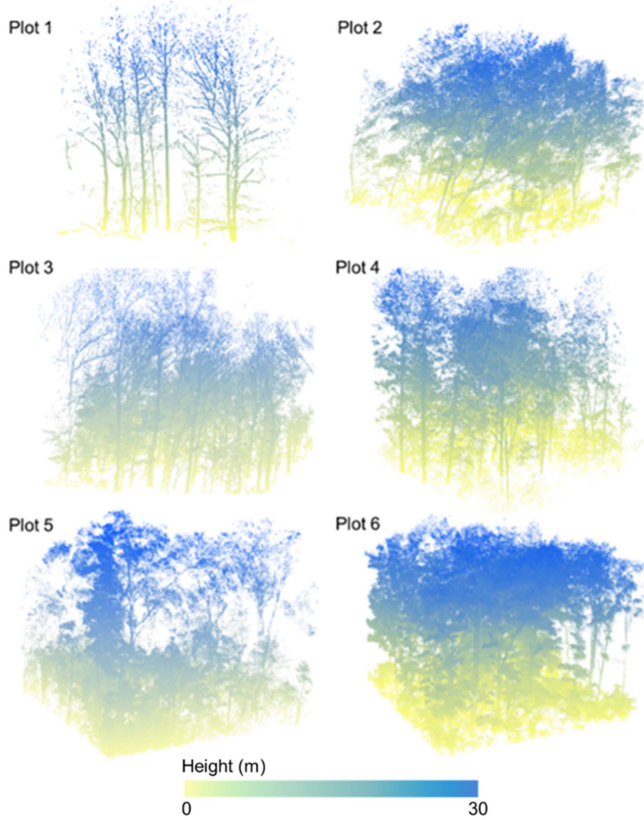


Fig. 1. Point clouds in each plot.

points caused by wind and multipath effects. Ground point filtering separated ground points from nonground points and improved progressive tin densification filtering method was adopted [31]. Normalization was done to eliminate the effect of terrain elevation on LiDAR height [32].

### C. Validation Data

We manually marked the locations of the individual trees via visual interpretation of the point cloud data, and later used them as seed points. The point cloud of each individual tree in the plot was obtained by using the “point cloud segmentation based on seed points” function of LiDAR360 software [33], [34]. The potential segmentation errors in the individual tree point cloud were then corrected by visual inspection. The results based on manual correction were used as reference data to evaluate the accuracy of the proposed segmentation method (Fig. 2).

## III. METHOD

The main principle of the proposed individual tree segmentation method is based on the centripetal relationship between the trunk and branches, which can be determined by calculating the directivity. As shown in Fig. 3, the growth of tree branches follows a certain topological structure, which shows a strong centripetal relation between the primary and secondary branches. Based on this structure, if the trunk of a tree is identified in the process of individual tree segmentation, all

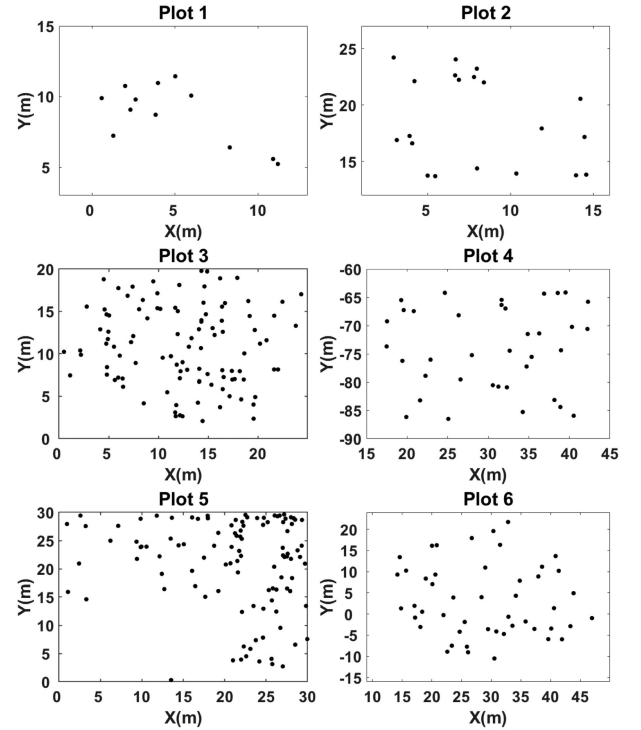


Fig. 2. Schematic diagram of the distribution of individual trees in the sample plot. Each black dot denotes one tree.

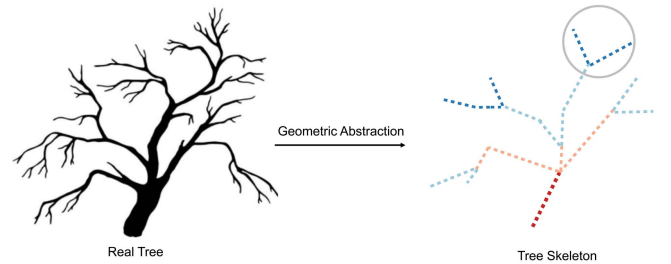


Fig. 3. Basic principle of the proposed algorithm. The tree skeleton is derived from geometric abstraction, and different levels of branches are depicted with different colors. Due to growth conditions constraints, the centripetal nature between nonadjacent levels of branches may not be evident (circled branch and the lowest branch).

the secondary branches corresponding can be identified based on the centripetal assessment. This process is iterated branch by branch to reconstruct the branch topology of an individual tree, providing strict geometric constraints for the individual tree segmentation, and enhancing the accuracy of the process.

Therefore, the strategy for individual tree segmentation can be divided into two major parts: branch point segmentation and leaf point segmentation (Fig. 4). The key step is branch segmentation, which consists of three parts: superpoint construction, branch detection, and directional clustering. A superpoint is defined as an aggregated representation of a geometrically meaningful portion of the point cloud, which is similar to a hypervoxel. The purpose of superpoint construction is to simply divide the original disordered point cloud into superpoint objects carrying entity semantic information, so that the directivity of the branch



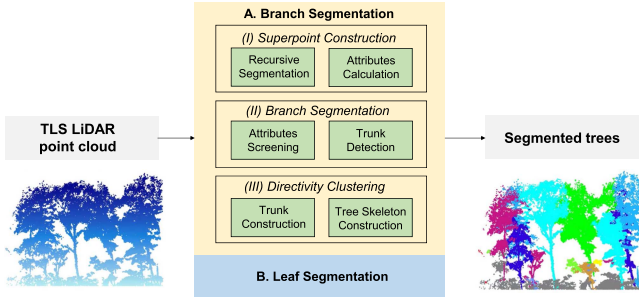


Fig. 4. Flow chart of the proposed individual tree segmentation method.

can be perfectly displayed on the superpoint scale rather than on the point scale. In addition, this step greatly reduces the scale of point cloud processing in the individual tree segmentation process, and increases the algorithm's efficiency. The branch detection aims at eliminating the influence of leaf points with no clear directionality and identifying points suitable for leaf point segmentation. In the directional clustering step, superpoints are iteratively merged according to the similarity of the calculated directionality, generating the tree skeleton segmentation results. After the branch segmentation, the nearest distance algorithm is used to complete the leaf point segmentation step and the leaf points are assigned to the segmented tree skeleton to obtain the final individual tree segmentation results.

#### A. Branch Segmentation

1) *Superpoint Construction*: The process of superpoint construction first divides the point cloud into geometrically simple parts to ensure semantic homogeneity. This means that each small point cluster only contains one type of objects and enough semantic information used for later directional calculation. According to Wang [29], a fully automatic graph-based segmentation is used to generate the superpoints. First, an undirected graph is constructed by using the adjacency relationship between points. Second, the adjacent edges of the graph are trimmed by adding the feature information of the point cloud. Only the connection between spatial adjacent points with similar features is preserved, and the graph is segmented according to these connections. Finally, a superpoint dataset  $S$  with homogeneous semantics is generated. Details of this segmentation method can be referred to Wang [29].

Then, feature information is calculated at the superpoint level. The information enriches the superpoint semantics and supports the branch detection step by providing attributes. The additional feature information consists of six dimensions: the number of point clouds, the center point, the lowest point, the highest point, the linearity, and the directivity (Table III).

For the superpoint belonging to  $S$ , the number of points  $N$  can be obtained by directly counting the number of points contained in the superpoint. The center point  $P_C$  can be obtained by directly calculating the gravity center of the superpoint. The lowest point  $P_L$  and the highest point  $P_H$  are acquired by arranging the points in the superpoint according to the  $z$  value. Then, the minimum  $z$  value point is selected as the  $P_L$ , while the maximum  $z$  value point is selected as the  $P_H$ . The linearity  $Li$  and the directivity

TABLE III  
ADDITIONAL FEATURE INFORMATION OF THE SUPERPOINT

Symbol	Description	Dimension
$N$	Number of points	1
$P_C$	Center point	3
$P_L$	Lowest point	3
$P_H$	Highest point	3
$Li$	Linearity	1
$Dir$	Directivity	3

The dimension value represents dimensions required to describe the feature.

TABLE IV  
PRESET PARAMETERS FOR THE PROPOSED METHOD

Symbol	Description	Value
$N_{\text{branch}}$	Branch point cloud number threshold	10
$Li_{\text{branch}}$	Branch linearity threshold	0.6
$N_{\text{trunk}}$	Trunk point cloud number threshold	100
$Li_{\text{trunk}}$	Trunk linearity threshold	0.8

$Dir$  can represent the linear features of the superpoint.  $Li$  can be derived from the largest eigenvalue in the covariance matrix of the superpoint and then is normalized between 0 and 1.  $Dir$  can be set as the unit eigenvector corresponding to the largest eigenvalue.

2) *Branch Detection*: During the long evolutionary process, the structure of trees has developed the most efficient way to transport water, in which cylindrical branches are used to maximize transport efficiency while using the least amount of material. Therefore, compared with the leaves, which are densely distributed to maximize light exposure, branches have more linear characteristics. This linear feature, represented as linearity  $Li$ , can help in the identification of the desired branch points. In addition, the number of points in the superpoint ( $N$ ) is also used in the screening process to eliminate small superpoint clustering with unclear directional features, reducing the amount of data processing and improving the efficiency of the algorithm.

Compared with tree canopies that overlap each other to compete for light, tree trunks are naturally separated from each other. Therefore, superpoints belonging to each trunk are naturally separated. Once the superpoints that belong to each trunk are found, they can be used as the representative location of each tree, and can be easily detected and applied to the following directivity clustering process as seed points. As the tree trunk is stronger and more linear than the branches, the linearity and the number of points can be used as screening indicators to directly obtain the superpoints belonging to the trunk. The threshold parameters need to be specified to obtain the optimal trunk seed point. Thus, parameters to determine the branch superpoint (i.e., the branch point cloud number threshold  $N_{\text{branch}}$  and the branch linearity threshold  $Li_{\text{branch}}$ ) and the trunk superpoint (i.e., the trunk point cloud number threshold  $N_{\text{trunk}}$  and trunk linearity threshold  $Li_{\text{trunk}}$ ) should be predetermined. The values and specific descriptions of all parameters involved in the experiment are shown in Table IV. We adopted the same parameter configuration in each plot.

3) *Directivity Clustering*: As the tree grows, the secondary branches only develop on higher branches. According to the topological structure of tree branches, the secondary branches of a tree are generally more centripetal than the upper branches, but weaker than the higher branches. Not establishing first the higher branches may lead to errors in attaching the secondary branches. Therefore, the trunk of the tree should be built first by determining the superpoints at 1.3 m that belong to the trunk and taking them as the seed superpoint set  $R$ . Then, the directivity clustering is operated to merge other trunk superpoints with the seed superpoints according to the centripetal condition. Here, the centripetal condition is defined as follows:

$$U(s_i, s_j) = U_{ij} = \begin{cases} 1, & \text{if } d_{ij} < r_i^* + r_j^* \\ 0, & \text{otherwise} \end{cases} \quad (1)$$

where  $U_{ij}$  denotes the centripetal condition between superpoint  $s_i$  and  $s_j$ .  $d_{ij}$  denotes the shortest vertical distance between the center line of superpoint  $s_i$  and  $s_j$  on the direction vector extension line. Approximate the trunk superpoints as a cylinder,  $r_1^*$  and  $r_2^*$  denote the radius of the superpoint  $s_i$  and  $s_j$ . These variables can be calculated as follows:

$$d_{ij} = \frac{|(\text{Dir}_i \times \text{Dir}_j) \cdot (C_j - C_i)|}{|\text{Dir}_i \times \text{Dir}_j|} \quad (2)$$

$$r_i^* = \operatorname{argmax}_{P_a, P_b \in s_i} \frac{|(P_a - P_b) \times \text{Dir}_i|}{|\text{Dir}_i|} \quad (3)$$

where  $\text{Dir}_i$  and  $\text{Dir}_j$  represent the directivity of superpoint  $s_i$  and  $s_j$ , respectively; and  $C_i$  and  $C_j$  represent the center point of  $s_i$  and  $s_j$ , respectively.  $P_a$  and  $P_b$  denote the point that belongs to the superpoint  $s_i$  and  $s_j$ .

The steps of directivity clustering are similar to regional growth. The process starts with a superpoint set  $S$  needed to be clustered and the seed superpoint set  $R$ . The superpoint set  $S$  is traversed to merge with the seed superpoints in order from lowest to highest in the  $z$  direction and calculated the centripetal condition with the seed superpoint from closest to farthest. The superpoint is classified to the tree which its satisfied and closest seed superpoint belongs to. Otherwise, the superpoint is added to  $S'$  which is initialized as an empty set before the process. The process is repeated until  $S'$  is empty. Before each epoch, the lowest superpoint in  $S'$  will be deleted and added to  $R$  as a new seed superpoint. Then,  $S$  will be set as  $S'$ , and  $S'$  will be initialized as an empty set again. The main steps are described in Algorithm 1.

Since the accuracy of directivity clustering is determined by the merging step, three points should be emphasized. First, because the branch superpoints are not continuously distributed in space, it is necessary to use the cylinder extension to determine whether the condition is satisfied. In other words, if the distance between the center lines of the two superpoints is less than the sum of the radius of the two cylinders, the two superpoints can be assumed to intersect (Fig. 5).

Second, in the process of evaluating the intersection relationship, it is possible for a trunk superpoint to intersect with multiple seed superpoints, resulting in a conflict with the basic principle that each branch must belong to only one tree. Since

---

**Algorithm 1: Directivity Clustering Algorithm.**


---

```

1: Input:
2:  $S = \{s_1, s_2, s_3, \dots, s_n\}$ : superpoint set needed to be clustered
3:  $R = \{r_1, r_2, r_3, \dots, r_m\}$ : seed superpoint set
4:  $Y = \{y_1, y_2, y_3, \dots, y_m\}$ : segmented superpoint set for each tree and  $y_i = \{r_i\}$ 
5:  $Z(\cdot)$ : the value in  $z$  direction of the point
6:  $C(\cdot)$ : the center point of the superpoint
7:  $U(\cdot)$ : the centripetal condition value of two superpoints
8: Output:
9: Reconstructed seed superpoint set:  $R = \{r_1, r_2, r_3, \dots, r_m, r_{m+1}, \dots, r_{m+k}\}$ 
10: Trunk segmentation results:  $Y_{\text{out}} = \{Y_1, Y_2, \dots, Y_m, Y_{m+1}, \dots, Y_{m+k}\}$ 
11: procedure Directivity clustering
12: Initialize  $S' = \emptyset$ 
13: while ( $S \neq S'$ ) do
14:    $s_z = \operatorname{argmin}_{s \in S'} Z(C(s))$ 
15:   for  $j = 1, 2, 3 \dots m$  do
16:     if  $U(s_z, r_j) = 1$  then
17:        $y_j = y_j \cup \{s_z\}$ 
18:     else
19:        $S' = S' \cup \{s_z\}$ 
20:   end for
21:   if  $S' \neq \emptyset$  then
22:     if  $S' \neq S$  then
23:        $S = S'$ 
24:        $S' = \emptyset$ 
25:     else
26:        $r = \operatorname{argmin}_{s \in S'} Z(C(s))$ 
27:        $R = R \cup \{r\}$ 
28:     end if
29:   else
30:     break
31:   end if
32: end while
    
```

---

the most efficient branch transport structure has formed through evolution, the plane distance between the branch and the tree seed point should be the closest when projecting to the ground. To simplify the calculation, the plane distance is determined between two center points in two superpoints. Then, the superpoint is attributed to the cluster the seed superpoint holds (Fig. 5).

Third, when a new superpoint is added to the cluster, the seed superpoint representing the cluster should be reconstructed. Since the orientation of the tree trunk may change continuously with the increase of  $z$  value, it is necessary to continuously change the seed point to correct the error caused by the change of orientation. Therefore, whenever a new superpoint  $S_i$  is added to a certain cluster, the merge of the current superpoint  $S_i$  and its closest seed superpoint  $R_j$  serve as a new superpoint. The attributes of this new superpoint are also calculated with the change (Fig. 6).

After the skeleton of the trunk is constructed, the remaining branches are merged with trunk superpoints in the process of

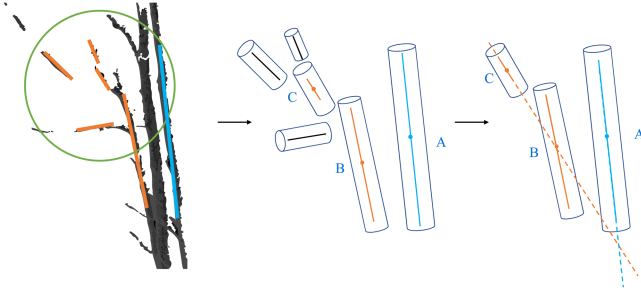


Fig. 5. Concept diagram of cylinder intersection decision. The original point cloud can be represented as superpoints whose shapes are cylinder. The intersection between superpoints can be determined by assessing the intersection between cylinders. The existence of multiple intersecting decisions is also given. Here, both A and B intersects with C, and C is determined to be merged with B since B is much closer.

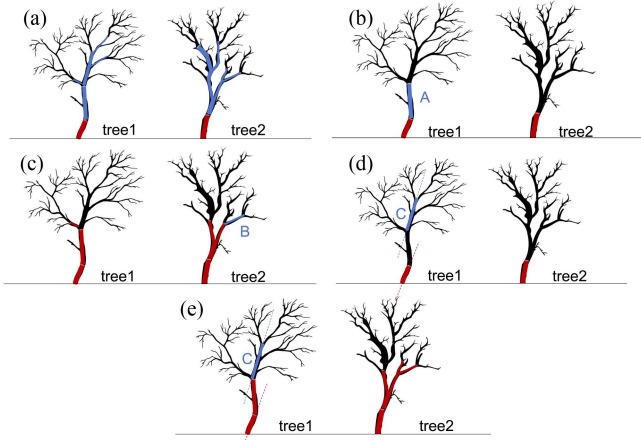


Fig. 6. Two trees are taken as an example to show the conceptual map of merging according to directivity. (a) Seed superpoint and the branch superpoint that need to be merged are marked in red and blue, respectively. (b) Superpoint A is classified as tree 1 since it only intersects with tree 1. (c) Superpoint B is classified as tree 2 because it is closer to tree 2 while it intersects with both tree 1 and tree 2. (d) Superpoint C is not classified as tree 1 if the seed point is not reconstructed. Superpoint C is classified as tree 1 if the reconstruction step is operated.

directivity clustering. Similar to the method of trunk construction in the previous section, the seed superpoints constructed before serve as the same seed set for the clustering process of the remaining superpoints. In this step, since the branch superpoints include the branches of different levels of the tree, to gradually reconstruct the branch topology relationship of a single tree, this step differs from the trunk construction step in two aspects.

First, the order of direction clustering is determined by the plane distance between the branches and the trunk, and the clustering is performed in order from closest to furthest. This is due to the fact that relatively high-level branches are closer to the trunk than the low-level branches. This order is conducive to strict geometric constraints for relatively low-level branches by adding relatively high-level branches to the cluster first.

Second, the seed point reconstruction steps should change. If the trunk superpoint and the low-level branch point are simply mixed together, the directivity of the tree branch is not reflected at all, which may lead to subsequent serious errors. Therefore,

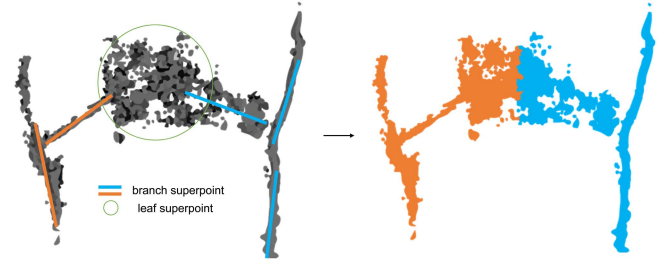


Fig. 7. Concept diagram of leaf segmentation. Black dots in leaf superpoint represent the leaf point obtained by TLS. If leaf segmentation is conducted at superpoint level, all leaf points would be attributed to only one tree. By conducting leaf segmentation at point level, the leaf point can be correctly assigned.

in the seed superpoint reconstruction step, it is necessary to establish seed superpoints for branch levels. The main steps are as follows. After obtaining the cluster the current superpoint  $s_i$  belongs to, the branch judgment condition is used to determine whether the seed superpoint of the current branch has been added in the seed superpoint set. If there is an existing seed superpoint  $r_k$ ,  $r_k$  and  $s_i$  are then combined to generate a new seed superpoint  $R'_k$  to replace the original seed point  $R_k$ . If not, the current superpoint is added to the set of seed superpoints as a new seed superpoint. The evaluation of the branch condition is as follows:

$$M_{ij} = \begin{cases} 1 & \text{if } \begin{cases} \alpha(\text{Dir}_i, \text{Dir}_j) < \frac{\pi}{6} \\ (C_i - C_j) \cdot \text{Dir}_j > 0 \end{cases} \\ 0, & \text{otherwise} \end{cases} \quad (4)$$

where  $M_{ij}$  represents the relationship between the current seed superpoint  $r_j$  and the current superpoint  $s_i$ . If  $M_{ij}$  reaches 1, then  $S_i$  and  $R_j$  belong to the same branch. Otherwise,  $s_i$  and  $r_j$  belong to different branches if  $M_{ij}$  reaches 0.  $\text{Dir}_i$  and  $\text{Dir}_j$  represent the directivity of  $s_i$  and  $r_j$ , respectively;  $\alpha$  then represents the angle between these two directivities; and  $C_i$  and  $C_j$  represent the center point of  $s_i$  and  $r_j$ , respectively. This condition means that if the directions of  $S_i$  and its intersecting seed superpoint  $r_j$  are similar, and  $S_i$  is completely in the extension direction of seed superpoint  $r_j$ , then they are considered to belong to the same branch of a tree.

### B. Leaf Segmentation

Since the leaves of each tree are attached to the branches, the leaves must be the closest to the branches to which they are attached. According to this rule, the shortest distance criterion can directly determine which tree the leaves belong to. It is worth noting that this step operates on the point scale instead of the superpoint scale. This is because the constructed superpoint may contain leaf point clouds of various trees with intersecting canopies. If the whole superpoint is simply attributed to a certain tree, the leaf points belonging to multiple trees may be incorrectly classified as one tree, causing severe leaf point segmentation errors. Therefore, in this step, the leaf superpoints are divided into leaf points at first, and then an iterative method is used to segment the leaf points (Fig. 7).

**Algorithm 2:** Leaf Segmentation Algorithm.

---

```

1: Input:
2:  $L = \{l_1, l_2, l_3, \dots, l_n\}$ : unclassified leaf point clouds
3:  $P = \{p_1, p_2, p_3, \dots, p_b\}$ : full point cloud
4:  $X = \{x_1, x_2, x_3, \dots, x_c\}$ : segmented point cloud set for
   each tree and segmented tree number is  $c$ 
5:  $d(\cdot)$ : the Euclidean distance between two points
6:  $\text{num}(\cdot)$ : the elements number of one set
7: Output:
8: Tree segmentation results:  $X = \{x_1, x_2, x_3, \dots, x_c\}$ 
9: procedure Leaf segmentation
10: Initialize  $L' = \emptyset$ 
11: while ( $L \neq \emptyset$ ) do
12:    $n = \text{num}(L)$ 
13:   for  $j = 1, 2, 3 \dots n$  do
14:      $p^* = \text{argmin}_{p \in P} d(l_j, p)$ 
15:     if  $\exists x_i, p^* \in x_i$  then
16:        $x_i = x_i \cup \{p^*\}$ 
17:     else
18:        $L' = L' \cup \{p^*\}$ 
19:     end if
20:   end for
21:    $L = L'$ 
22: end while

```

---

This process can be interpreted as follows. Also unclassified leaf point clouds  $L$  and an empty set  $L'$  are initialized. The leaf point is then traversed in the order of distance from closest to furthest and classified to a certain tree which its adjacent point belongs to. When its adjacent point is not classified, the point is added to  $L'$ . This step is repeated until the  $L'$  is empty. Before each epoch,  $L$  will be set as  $L'$  and  $L'$  will be initialized as an empty set again. And basic process is described in Algorithm 2 as follows.

### C. Evaluation

By combining topology information with superpoints, the method is improved and suitable for more types of forests. To further show our improvements in this method, a comparison of the original superpoint algorithm was carried out over the experimental plots. For the original algorithm, the optimal parameters were used according to the literature to obtain the best individual tree segmentation results [35]. In addition, another widely used individual tree segmentation based on ecological theory, namely the ecological method [30], which was integrated into LiDAR360 software (Green Valley International), was also compared with the proposed method. The recommended parameters were also adopted for different plots to obtain the individual tree segmentation results according to the user manual (Green Valley International).

Three types of tree segments and corresponding levels of accuracy are produced. True positive (TP) refers to the correctly segmented tree. False negative or omission error refers to the tree, which is not segmented and assigned to its nearby tree. False positive or commission error takes place when a tree does not exist but wrongly segmented. The higher the value of TP

is, the better performance this method holds. In this article, recall ( $r$ ), precision ( $p$ ), and  $F$ -score were calculated to assess the accuracies. The definitions are as follows:

$$r = \frac{\text{TP}}{\text{TP} + \text{FN}} \quad (5)$$

$$p = \frac{\text{TP}}{\text{TP} + \text{FP}} \quad (6)$$

$$F = \frac{r \times p}{r + p} \times 2. \quad (7)$$

In addition to the assessment at the tree scale, an accuracy assessment at the point scale was also completed. The confusion matrix  $A$  and the index intersection over union (IoU) were calculated for the assessment. Each value  $A_{ij}$  in this matrix indicates the number of points that belong to tree  $i$  but clustered to tree  $j$ . The original definition of IoU is the intersection area versus the union area between the two. When migrating to the point cloud, it can be defined as the number of intersection points versus the number of union points. The IOU of the tree  $i$  can be calculated by the following formula:

$$\text{IoU}_i = \frac{A_{ii}}{A_{ii} + \sum_{j \neq i} A_{ij} + \sum_{k \neq i} A_{ki}}. \quad (8)$$

Then, the average IoU of all trees can be calculated using the following formula:

$$m\text{IoU} = \frac{\sum_{i=1}^N \text{IoU}_i}{N} \quad (9)$$

where  $N$  represents the number of trees.

Overall accuracy (OA) can be calculated by using the confusion matrix:

$$\text{OA} = 100\% \times \frac{\sum_{i=1}^N A_{ii}}{\sum_{j=1}^N \sum_{k=1}^N A_{jk}}. \quad (10)$$

## IV. RESULTS

### A. Evaluation at Tree Level

The accuracy of tree-level segmentation results is shown in Table V. In addition, the segmentation results of each tree are displayed in detail on the sample plot (Fig. 7). In plot 1, which is mainly composed of tree trunk point clouds, the algorithm proposed in this article can identify all trees without commission and omission errors. The scores of  $r$ ,  $p$ , and  $F$ -score are higher than those of the other two algorithms. Compared with the superpoint algorithm and the ecological method, the algorithm in this article is also better at extracting tree trunks, with the accuracy measured by the  $F$ -score improved by 25% and 10%, respectively. In the planted coniferous forest plot 2, the proposed algorithm still has an advantage in  $r$ , and the accuracy measured by the  $F$ -score is increased by 30% and 6%, respectively, while the segmentation accuracy obtained by the original superpoint method and the ecological method is lower.

The results reported in plots 3 and 4 show also best  $r$  for the proposed method, noticeably higher than the original superpoint method and also slightly higher than the ecological method by about 2% and 1%, respectively. But the value of  $p$  is still not as



TABLE V  
ACCURACY ASSESSMENT OF THE SEGMENTATION AT THE TREE LEVEL

Plot	Method	Number of reference trees	Number of segmented trees	TP	FP	FN	$r$	$p$	$F$ -score
1	Ecological method	11	11	10	1	1	0.909	0.909	0.909
	Original superpoint	11	9	8	1	3	0.727	0.889	0.800
	Proposed method	11	11	11	<b>0</b>	<b>0</b>	<b>1.000</b>	<b>1.000</b>	<b>1.000</b>
2	Ecological method	20	14	13	1	7	0.650	0.929	0.765
	Original superpoint	20	9	9	<b>0</b>	11	0.450	<b>1.000</b>	0.621
	Proposed method	20	22	<b>17</b>	5	<b>3</b>	<b>0.850</b>	0.773	<b>0.810</b>
3	Ecological method	114	109	101	13	<b>8</b>	0.886	0.927	<b>0.906</b>
	Original superpoint	114	76	73	<b>3</b>	38	0.640	<b>0.961</b>	0.800
	Proposed method	114	126	<b>102</b>	24	12	<b>0.895</b>	0.810	0.833
4	Ecological method	37	39	<b>30</b>	9	<b>7</b>	0.811	0.769	<b>0.789</b>
	Original superpoint	37	15	15	<b>0</b>	22	0.405	<b>1.000</b>	0.577
	Proposed method	37	42	31	11	6	<b>0.838</b>	0.738	0.785
5	Ecological method	109	165	74	91	<b>25</b>	0.679	0.448	0.540
	Original superpoint	109	7	7	<b>0</b>	102	0.064	1.000	0.121
	Proposed method	109	106	<b>76</b>	30	33	0.697	0.717	<b>0.707</b>
6	Ecological method	48	55	<b>45</b>	10	<b>3</b>	<b>0.938</b>	0.818	<b>0.874</b>
	Original superpoint	48	4	4	<b>0</b>	44	0.083	<b>1.000</b>	0.154
	Proposed method	48	59	32	27	16	0.667	0.542	0.598

The best values in each plot are presented in bold form.

good as the ecological method, slightly worse than the ecological method, resulting in lower  $F$ -score in plot 4. Nevertheless, the proposed method greatly increases its  $r$  at the expense of some  $p$  and shows better results than the original superpoint method. In the broad-leaved forest plots 5 and 6 with more complicated forest conditions, the proposed method produces more commission errors, reaching 30 and 27 trees, respectively. The  $F$ -score is not as high as that of the ecological method. Compared with the original superpoint method, this proposed algorithm has greatly improved the number of recognized trees, with the accuracy measured by  $F$ -score increased by at least 36%.

As shown in Fig. 8, the proposed method generally produces more commission errors near the real trees. And its omission errors are distributed mainly in the place where two or more trees are crowded in a small area. Compared with the original superpoint method, the proposed method can tell more trees in areas with high tree density, such as plot 3 and plot 5. The ecological method generates similar commission errors as the proposed method but these errors would be less and distributed farther from the real trees.

### B. Evaluation at Point Level

For the segmentation results at the point level (Table VI), compared with the original superpoint algorithm, the proposed algorithm in this article has advantages in each sample plot with about 114% and 70% increased values of mIoU and OA, respectively. This is consistent with the previous segmentation results at the tree level. However, compared with the ecological method, the algorithm in this article only obtains the highest OA on sample plot 1, while the OA and mIoU on the other three sample plots are lower.

For the graphical results of the segmentation of each plot (Fig. 9), compared with the superpoint and ecological methods, the branches segmented by the algorithm in this article are more in line with the topological structure of tree branches. The segmentation results of plot 1 to plot 4 show that the algorithm in this article can clearly describe the extended branches of trees. The branches of each tree are continuous and similar branches can be segmented. It is worth noting that the algorithm in this article has a good description of the intersecting branches. At the position of the intersecting branches in plot 1 (such as the two trees on the left in Fig. 8), the segmentation results of the superpoint

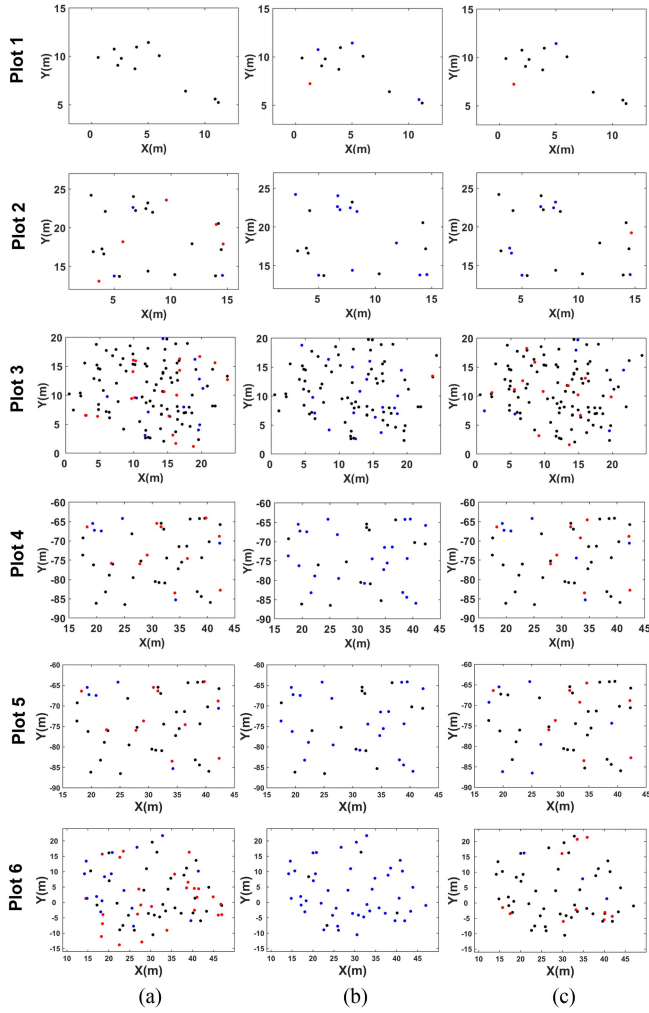


Fig. 8. Segmentation results in each plot. a, b, and c represent results of the proposed method, original superpoint method, and ecological segmentation method, respectively. The black, red, and blue dots refer to true positive (TP), false positive (FP), and false negative (FN), respectively.

algorithm and the ecological method show that the intersecting branches were simply assigned to the two trees according to the shortest distance. Nevertheless, the algorithm proposed in this article successfully distinguished the intersecting branches using the centrality of the branches, which also results in the highest OA in plot 1.

In plots 5 and 6, it is clear that due to the limited number of correctly segmented seed points, many branches are incorrectly connected to more distant seed points, resulting in lower segmentation accuracy.

### C. Parameters of the Proposed Algorithm

Due to the lack of validation data for individual tree branches, in this part only the two parameters determining the trunk superpoint, i.e.,  $N_{\text{trunk}}$  and  $L_{\text{trunk}}$ , are analyzed. Therefore, in this article, by adjusting the value of a single parameter at a constant interval while keeping other parameter values unchanged, the change of the  $F$ -score of the tree-level results of individual tree segmentation with parameter changes was analyzed in Plot 2.

TABLE VI  
ACCURACY ASSESSMENT OF THE SEGMENTATION AT THE POINT LEVEL

Plot	Method	mIoU	OA
1	Original superpoint	0.535	0.550
	Proposed method	<b>0.787</b>	<b>0.804</b>
2	Original superpoint	0.395	0.538
	Proposed method	<b>0.582</b>	<b>0.625</b>
3	Original superpoint	0.409	0.498
	Proposed method	<b>0.428</b>	<b>0.545</b>
4	Original superpoint	0.263	<b>0.418</b>
	Proposed method	<b>0.289</b>	0.371
5	Original superpoint	0.090	0.247
	Proposed method	<b>0.297</b>	<b>0.474</b>
6	Original superpoint	0.013	0.028
	Proposed method	<b>0.174</b>	<b>0.276</b>

The best values in each plot are presented in bold form.

As shown in Fig. 10, the method proposed in this article is not sensitive to  $N_{\text{trunk}}$ . The  $F$ -score fluctuates around 0.8 and may decrease in extreme cases with the change of parameters. The best results can be achieved by determining moderate parameters because a too-low threshold would cause overidentification in some secondary branches that do not belong to the trunk and a too-high threshold would cause some qualified trunk superpoints to be omitted, which would greatly increase the omission errors of the results.

Different from the parameter  $N_{\text{trunk}}$ ,  $L_{\text{trunk}}$  can significantly affect the accuracy of the proposed method, causing more fluctuations of the  $F$ -score in extreme cases. Relatively accurate results can be achieved when the trunk linearity threshold is slightly higher than the branch linearity threshold. In the same way, either too low or too high thresholds would lead to worse results. A moderate threshold used would guarantee good results. For different forest plots, the above two parameters can obtain the best results by simply repeating the experiment.

## V. DISCUSSION

Compared with the original algorithm, our algorithm mainly focuses on reconstructing the tree skeleton structure using ecological theory. This use of ecological theory has shown to be very effective in previous articles and has again been proven effective here [30], [36]. Taking into account the directivity

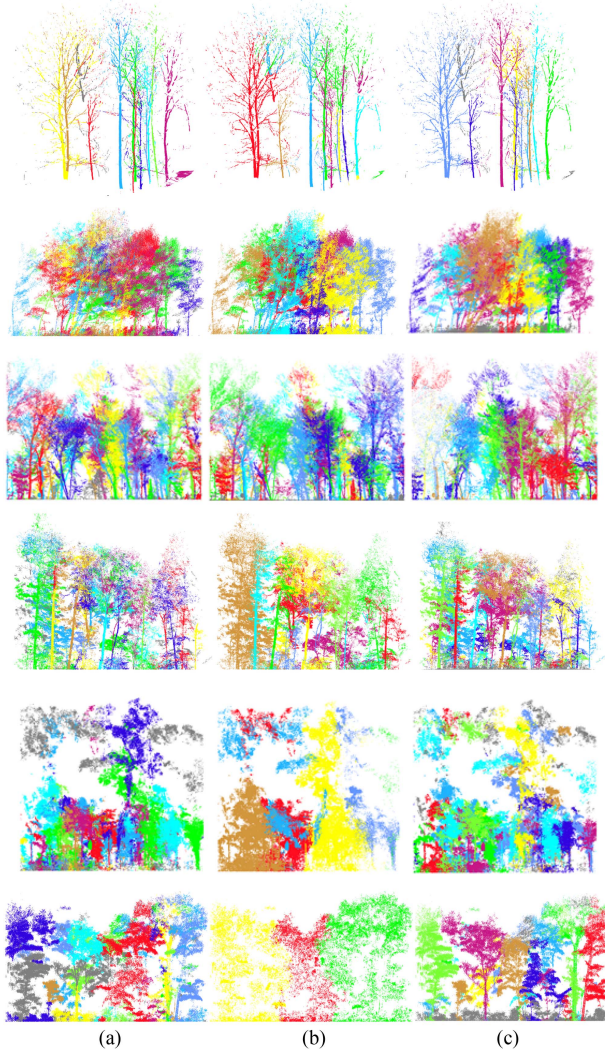


Fig. 9. Segmentation results in plot 1, 2, 3, 4, 5, and 6 are listed in order from top to bottom. (a), (b), and (c) represent the proposed method, the original superpoint method, and the ecological method, respectively.

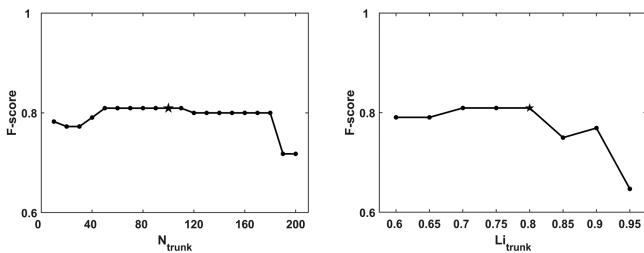


Fig. 10. Sensitivity analysis of preset parameters (the preset values used in this article are indicated by the black five-pointed star), where  $N_{trunk}$  and  $Li_{trunk}$  are the threshold of the number of the trunk point clouds and the threshold of trunk linearity, respectively.

between branches has greatly reduced the misclassification of different branches to other trees, resulting in improved accuracy. In addition, this algorithm simplifies the trunk skeleton construction, making the entire method easier and more practical.

Regarding sample plots with simple forest conditions, the proposed method can produce higher accuracy, as it is difficult

for the other two algorithms to distinguish trees with the same root point but separated branches [37]. The proposed algorithm can split trees more precisely through the separation relationship between branches. For complicated forest conditions, branches that do not intersect with bushes can be extracted during the directivity segmentation process [38], [39]. Thus, the tree trunks missed in the superpoint algorithm can be regenerated during the directional clustering process. This is the advantage of our algorithm based on the ecological tree centrality theory and expands the generality of this algorithm in different forest types.

Since our algorithm is dedicated for complicated forest conditions with dense low vegetations blocking the trunk, the complexity of tree trunks could also influence the accuracy of our algorithm. For multitruck trees, the algorithm could identify part of the tree trunks and treat them as different trunks. If the trees are with the same root, the results would be different when the tree bifurcates at different height, such as the results in plot 1. However, when trees are with different roots but share part of the same trunk, the algorithm would always integrate these trees. This is because this part of trunk would be clustered to impartible superpoints. And in the section directivity clustering, these superpoints would be treated as one tree and combines the root superpoints. In future articles, adding rules based on this ecological topology would improve our algorithm, which would help us gain more accurate individual trees under these conditions.

In this algorithm, four parameters have been determined to simplify the branch and trunk detection process. In this way, a large number of nondirectional superpoints are filtered out, and directivity clustering can be operated effectively without noise superpoints. Thus, these four parameters are of great importance. After a large number of experiments, for most forest types, the recommended values for  $N_{trunk}$  and  $Li_{trunk}$  are 100 and 0.8, respectively, while the recommended values for  $N_{branch}$  and  $Li_{branch}$  are 50 and 0.6. Most directional superpoints can be screened based on recommended thresholds. If these thresholds are not suitable and the commission errors are too high, they can be adjusted by adding 10 at the time, and the linearity thresholds can be adjusted by adding 0.05. Conversely, if omission errors are not acceptable, the number thresholds and linearity thresholds can be reduced by a certain value according to the same operation proposed. In this way, good segmentation results can be achieved.

After years of development, more and more methods and toolkits were developed for individual tree segmentation using TLS point clouds [17], [37], [40]. With the rapid development of computer vision, some classic algorithms like clustering are widely used [41]. Nevertheless, due to the complexity of the forest scene itself, dense low vegetation and complex terrain conditions have greatly affected the data quality, which may lead to the failure of some clustering methods based on computer vision in complicated forest plots [13]. Making use of the topology of the single tree and taking individual tree segmentation as a semantic segmentation task would help reconstruct single trees from complicated scene [42]. Past article and this article have once again confirmed that the semantic segmentation method combined with ecological theory can segment individual trees



more effectively in complicated scenes [38], [43], and [44]. Compared with other methods based on ecological theory, our method reconstructs the tree topology by using the centripetal nature of tree trunks and branches, which would have a unique ability to segment and identify shrubs. Future articles can also evaluate the uncertainty of the more advanced attributes obtained by the individual trees using our algorithm [10], [16], [45], [46].

However, results based on our algorithm do not meet our expectations for their low mIoU and OA. Furthermore, in some complicated forest conditions, the tree-level metrics are worse than the ecological method. This can be attributed to distance based superpoints construction method. Distance correction alone, without any other geometric constraints, cannot guarantee that superpoints adequately reflect the branch structure. During the superpoint construction process, when the bottom bush and the trunk are overlapped with each other, some bush points and trunk points will be allocated to the same superpoint, which is more difficult to distinguish in the branch detection process, resulting in more commission errors. Moreover, the threshold selection mainly depends on empirical attempts that would definitely introduce more uncertainty. The best threshold often leads to a large number of superpoints, greatly reducing efficiency. Also, too many superpoints would not perfectly reflect the skeleton structure. On this condition, two filtered thresholds, linearity and number, may be not enough for filtering the trunk and branch superpoints, such as the results in Changbai Mountain. Introducing high-dimensional geometric constrain may help solve this problem [47]. Besides, introducing more information like fusing airborne laser scanning would help generate less interference in the canopy [48]. In future articles, fixed-shape superpoints would better reflect the geometry of the tree, thus leading to better results.

## VI. CONCLUSION

In this article, we propose a novel approach to individual tree segmentation for TLS data by utilizing the topology of their branches. The proposed method involves the iterative construction of the individual tree point cloud based on the centripetal rule. The method has been tested in six sample plots with different forest complexities. Results show that the proposed method had significant improvements in both simple and complicated forest conditions compared with the original method, with an accuracy improvement of at least 36%. Compared with other existing individual tree segmentation methods suitable for forest environments, our method provides a better depiction of the tree branch structure, with an average improvement in accuracy of about 70%, which is a further improvement of existing superpoint segmentation methods. In addition, the analysis of the influence of parameter settings shows that the method is relatively robust, and the selection of appropriate parameters can ensure high accuracy of individual tree segmentations. Users can obtain the optimal parameter values through trial-and-error approach. In summary, the individual tree segmentation method proposed in this article is effective for complicated forest environments, providing valuable technical support for the extraction of individual trees under different forest conditions.

## REFERENCES

- [1] I. Oveland, M. Hauglin, T. Gobakken, E. Næsset, and I. Maalen-Johansen, "Automatic estimation of tree position and stem diameter using a moving terrestrial laser scanner," *Remote Sens.*, vol. 9, no. 4, 2017, Art. no. 350, doi: [10.3390/rs9040350](https://doi.org/10.3390/rs9040350).
- [2] J. Hyypä, H. Hyypä, M. Inkinen, M. Engdahl, S. Linko, and Y.-H. Zhu, "Accuracy comparison of various remote sensing data sources in the retrieval of forest stand attributes," *Forest Ecol. Manage.*, vol. 128, no. 1, pp. 109–120, 2000, doi: [10.1016/S0378-1127\(99\)00278-9](https://doi.org/10.1016/S0378-1127(99)00278-9).
- [3] R. N. Treuhaf and P. R. Siqueira, "Vertical structure of vegetated land surfaces from interferometric and polarimetric radar," *Radio Sci.*, vol. 35, no. 1, pp. 141–177, 2000, doi: [10.1029/1999RS900108](https://doi.org/10.1029/1999RS900108).
- [4] T. Brandtberg and F. Walter, "Automated delineation of individual tree crowns in high spatial resolution aerial images by multiple-scale analysis," *Mach. Vis. Appl.*, vol. 11, no. 2, pp. 64–73, 1998, doi: [10.1007/s001380050091](https://doi.org/10.1007/s001380050091).
- [5] K. Klasing, D. Wollherr, and M. Buss, "A clustering method for efficient segmentation of 3D laser data," in *Proc. IEEE Int. Conf. Robot. Automat.*, 2008, pp. 4043–4048, doi: [10.1109/ROBOT.2008.4543832](https://doi.org/10.1109/ROBOT.2008.4543832).
- [6] J. F. Weishampel, J. B. Blair, R. G. Knox, R. Dubayah, and D. B. Clark, "Volumetric lidar return patterns from an old-growth tropical rainforest canopy," *Int. J. Remote Sens.*, vol. 21, no. 2, pp. 409–415, 2000, doi: [10.1080/014311600210939](https://doi.org/10.1080/014311600210939).
- [7] P. Hyde et al., "Mapping forest structure for wildlife habitat analysis using waveform lidar: Validation of montane ecosystems," *Remote Sens. Environ.*, vol. 96, no. 3, pp. 427–437, 2005, doi: [10.1016/j.rse.2005.03.005](https://doi.org/10.1016/j.rse.2005.03.005).
- [8] H. Lee, K. C. Slatton, B. E. Roth, and W. P. Cropper, "Adaptive clustering of airborne LiDAR data to segment individual tree crowns in managed pine forests," *Int. J. Remote Sens.*, vol. 31, no. 1, pp. 117–139, 2010, doi: [10.1080/01431160902882561](https://doi.org/10.1080/01431160902882561).
- [9] P. Pueschel, G. Newnham, G. Rock, T. Udelhoven, W. Werner, and J. Hill, "The influence of scan mode and circle fitting on tree stem detection, stem diameter and volume extraction from terrestrial laser scans," *ISPRS J. Photogrammetry Remote Sens.*, vol. 77, pp. 44–56, 2013, doi: [10.1016/j.isprsjprs.2012.12.001](https://doi.org/10.1016/j.isprsjprs.2012.12.001).
- [10] N. Saarinen et al., "Assessing the effects of thinning on stem growth allocation of individual Scots pine trees," *Forest Ecol. Manage.*, vol. 474, 2020, Art. no. 118344, doi: [10.1016/j.foreco.2020.118344](https://doi.org/10.1016/j.foreco.2020.118344).
- [11] M. A. Lefsky, W. B. Cohen, G. G. Parker, and D. J. Harding, "Lidar remote sensing for ecosystem studies: Lidar, an emerging remote sensing technology that directly measures the three-dimensional distribution of plant canopies, can accurately estimate vegetation structural attributes and should be of particular interest to forest, landscape, and global ecologists," *BioScience*, vol. 52, no. 1, pp. 19–30, 2002, doi: [10.1641/0006-3568\(2002\)052\[0019:LRSFES\]2.0.CO;2](https://doi.org/10.1641/0006-3568(2002)052[0019:LRSFES]2.0.CO;2).
- [12] T. Yun et al., "Individual tree crown segmentation from airborne LiDAR data using a novel Gaussian filter and energy function minimization-based approach," *Remote Sens. Environ.*, vol. 256, 2021, Art. no. 112307, doi: [10.1016/j.rse.2021.112307](https://doi.org/10.1016/j.rse.2021.112307).
- [13] K. Calders et al., "Terrestrial laser scanning in forest ecology: Expanding the horizon," *Remote Sens. Environ.*, vol. 251, 2020, Art. no. 112102, doi: [10.1016/j.rse.2020.112102](https://doi.org/10.1016/j.rse.2020.112102).
- [14] Q. Guo et al., "Advances for the new remote sensing technology in ecosystem ecology research," *Chin. J. Plant Ecol.*, vol. 44, no. 4, pp. 418–435, 2020. [Online]. Available: <https://www.plant-ecology.com>
- [15] X. Liang et al., "Terrestrial laser scanning in forest inventories," *ISPRS J. Photogrammetry Remote Sens.*, vol. 115, pp. 63–77, 2016, doi: [10.1016/j.isprsjprs.2016.01.006](https://doi.org/10.1016/j.isprsjprs.2016.01.006).
- [16] M. Åkerblom, P. Raunonen, R. Mäkipää, and M. Kaasalainen, "Automatic tree species recognition with quantitative structure models," *Remote Sens. Environ.*, vol. 191, pp. 1–12, 2017, doi: [10.1016/j.rse.2016.12.002](https://doi.org/10.1016/j.rse.2016.12.002).
- [17] S. Krisanski et al., "Forest structural complexity tool—An open source, fully-automated tool for measuring forest point clouds," *Remote Sens.*, vol. 13, no. 22, 2021, Art. no. 4677, doi: [10.3390/rs13224677](https://doi.org/10.3390/rs13224677).
- [18] B. Wu, G. Zheng, Y. Chen, and D. Yu, "Assessing inclination angles of tree branches from terrestrial laser scan data using a skeleton extraction method," *Int. J. Appl. Earth Observ. Geoinf.*, vol. 104, 2021, Art. no. 102589, doi: [10.1016/j.jag.2021.102589](https://doi.org/10.1016/j.jag.2021.102589).
- [19] P. Zhao, L. Gao, and T. Gao, "Extracting forest parameters based on stand automatic segmentation algorithm," *Sci. Rep.*, vol. 10, no. 1, Jan. 2020, Art. no. 1571, doi: [10.1038/s41598-020-58494-6](https://doi.org/10.1038/s41598-020-58494-6).
- [20] H. Guan et al., "A marker-free method for registering multi-scan terrestrial laser scanning data in forest environments," *ISPRS J. Photogrammetry Remote Sens.*, vol. 166, pp. 82–94, 2020, doi: [10.1016/j.isprsjprs.2020.06.002](https://doi.org/10.1016/j.isprsjprs.2020.06.002).



- [21] W. Li, Q. Guo, M. K. Jakubowski, and M. Kelly, "A new method for segmenting individual trees from the lidar point cloud," *Photogrammetric Eng. Remote Sens.*, vol. 78, no. 1, pp. 75–84, 2012, doi: [10.14358/PERS.78.1.75](https://doi.org/10.14358/PERS.78.1.75).
- [22] Q. Yang et al., "The influence of vegetation characteristics on individual tree segmentation methods with airborne LiDAR data," *Remote Sens.*, vol. 11, no. 23, Art. no. 2880, doi: [10.3390/rs11232880](https://doi.org/10.3390/rs11232880).
- [23] M. P. Ferreira et al., "Individual tree detection and species classification of Amazonian palms using UAV images and deep learning," *Forest Ecol. Manage.*, vol. 475, 2020, Art. no. 118397, doi: [10.1016/j.foreco.2020.118397](https://doi.org/10.1016/j.foreco.2020.118397).
- [24] B. Hu, J. Li, L. Jing, and A. Judah, "Improving the efficiency and accuracy of individual tree crown delineation from high-density LiDAR data," *Int. J. Appl. Earth Observ. Geoinf.*, vol. 26, pp. 145–155, 2014, doi: [10.1016/j.jag.2013.06.003](https://doi.org/10.1016/j.jag.2013.06.003).
- [25] L. Huo, E. Lindberg, and J. Holmgren, "Towards low vegetation identification: A new method for tree crown segmentation from LiDAR data based on a symmetrical structure detection algorithm (SSD)," *Remote Sens. Environ.*, vol. 270, 2022, Art. no. 112857, doi: [10.1016/j.rse.2021.112857](https://doi.org/10.1016/j.rse.2021.112857).
- [26] N. Amiri, *Assessment of Marker-Controlled Watershed Segmentation Algorithm for Individual Tree Top Detection and Crown Delineation*. Enschede, The Netherlands: Univ. Twente, 2014.
- [27] J. Holmgren and E. Lindberg, "Tree crown segmentation based on a tree crown density model derived from airborne laser scanning," *Remote Sens. Lett.*, vol. 10, no. 12, pp. 1143–1152, 2019, doi: [10.1080/2150704X.2019.1658237](https://doi.org/10.1080/2150704X.2019.1658237).
- [28] A. M. Ramiya, R. R. Nidamanuri, and R. Krishnan, "Individual tree detection from airborne laser scanning data based on supervoxels and local convexity," *Remote Sens. Appl.: Soc. Environ.*, vol. 15, 2019, Art. no. 100242, doi: [10.1016/j.rsase.2019.100242](https://doi.org/10.1016/j.rsase.2019.100242).
- [29] D. Wang, "Unsupervised semantic and instance segmentation of forest point clouds," *ISPRS J. Photogrammetry Remote Sens.*, vol. 165, pp. 86–97, 2020, doi: [10.1016/j.isprsjprs.2020.04.020](https://doi.org/10.1016/j.isprsjprs.2020.04.020).
- [30] S. Tao et al., "Segmenting tree crowns from terrestrial and mobile LiDAR data by exploring ecological theories," *ISPRS J. Photogrammetry Remote Sens.*, vol. 110, pp. 66–76, 2015, doi: [10.1016/j.isprsjprs.2015.10.007](https://doi.org/10.1016/j.isprsjprs.2015.10.007).
- [31] X. Zhao, Q. Guo, Y. Su, and B. Xue, "Improved progressive TIN densification filtering algorithm for airborne LiDAR data in forested areas," *ISPRS J. Photogrammetry Remote Sens.*, vol. 117, pp. 79–91, 2016, doi: [10.1016/j.isprsjprs.2016.03.016](https://doi.org/10.1016/j.isprsjprs.2016.03.016).
- [32] Q. Guo et al., "Lidar boosts 3D ecological observations and modelings: A review and perspective," *IEEE Geosci. Remote Sens. Mag.*, vol. 9, no. 1, pp. 232–257, Mar. 2021, doi: [10.1109/MGRS.2020.3032713](https://doi.org/10.1109/MGRS.2020.3032713).
- [33] B. G. Weinstein, S. Marconi, S. Bohlman, A. Zare, and E. White, "Individual tree-crown detection in RGB imagery using semi-supervised deep learning neural networks," *Remote Sens.*, vol. 11, no. 11, 2019, Art. no. 1309.
- [34] X. Xu, F. Iuricich, K. Calders, J. Armston, and L. De Floriani, "Topology-based individual tree segmentation for automated processing of terrestrial laser scanning point clouds," *Int. J. Appl. Earth Observ. Geoinf.*, vol. 116, 2023, Art. no. 103145, doi: [10.1016/j.jag.2022.103145](https://doi.org/10.1016/j.jag.2022.103145).
- [35] D. Wang, S. M. Takoudjou, and E. Casella, "LeWoS: A universal leaf-wood classification method to facilitate the 3D modelling of large tropical trees using terrestrial LiDAR," *Methods Ecol. Evol.*, vol. 11, no. 3, pp. 376–389, 2020, doi: [10.1111/2041-210X.13342](https://doi.org/10.1111/2041-210X.13342).
- [36] Q. Liu, W. Ma, J. Zhang, Y. Liu, D. Xu, and J. Wang, "Point-cloud segmentation of individual trees in complex natural forest scenes based on a trunk-growth method," *J. Forestry Res.*, vol. 32, no. 6, pp. 2403–2414, 2021, doi: [10.1007/s11676-021-01303-1](https://doi.org/10.1007/s11676-021-01303-1).
- [37] N. Norzaki and K. N. Tahar, "A comparative study of template matching, ISO cluster segmentation, and tree canopy segmentation for homogeneous tree counting," *Int. J. Remote Sens.*, vol. 40, no. 19, pp. 7477–7499, 2018, doi: [10.1080/01431161.2018.1524182](https://doi.org/10.1080/01431161.2018.1524182).
- [38] D. Wang, X. Liang, G. Mofack, and O. Martin-Ducup, "Individual tree extraction from terrestrial laser scanning data via graph pathing," *Forest Ecosyst.*, vol. 8, 2021, Art. no. 67, doi: [10.1186/s40663-021-00340-w](https://doi.org/10.1186/s40663-021-00340-w).
- [39] X. Liang et al., "International benchmarking of terrestrial laser scanning approaches for forest inventories," *ISPRS J. Photogrammetry Remote Sens.*, vol. 144, pp. 137–179, 2018, doi: [10.1016/j.isprsjprs.2018.06.021](https://doi.org/10.1016/j.isprsjprs.2018.06.021).
- [40] A. Burt, M. Disney, K. Calders, and S. Goslee, "Extracting individual trees from lidar point clouds using treeseg," *Methods Ecol. Evol.*, vol. 10, pp. 438–445, 2018, doi: [10.1111/2041-210X.13121](https://doi.org/10.1111/2041-210X.13121).
- [41] J. Trochta, M. Kruczek, T. Vrska, and K. Kral, "3D Forest: An application for descriptions of three-dimensional forest structures using terrestrial LiDAR," *PLoS One*, vol. 12, no. 5, 2017, Art. no. e0176871, doi: [10.1371/journal.pone.0176871](https://doi.org/10.1371/journal.pone.0176871).
- [42] Y. Dong, Z. Ma, F. Xu, and F. Chen, "Unsupervised semantic segmenting TLS data of individual tree based on smoothness constraint using open-source datasets," *IEEE Trans. Geosci. Remote Sens.*, vol. 60, 2022, Art. no. 4415615, doi: [10.1109/tgrs.2022.3218442](https://doi.org/10.1109/tgrs.2022.3218442).
- [43] L. Chang, H. Fan, N. Zhu, and Z. Dong, "A two-stage approach for individual tree segmentation from TLS point clouds," *IEEE J. Sel. Topics Appl. Earth Observ. Remote Sens.*, vol. 15, pp. 8682–8693, 2022, doi: [10.1109/jstars.2022.3212445](https://doi.org/10.1109/jstars.2022.3212445).
- [44] X. Xu, F. Iuricich, K. Calders, J. Armston, and L. De Floriani, "Topology-based individual tree segmentation for automated processing of terrestrial laser scanning point clouds," *Int. J. Appl. Earth Observ. Geoinf.*, vol. 116, 2023, Art. no. 103145, doi: [10.1016/j.jag.2022.103145](https://doi.org/10.1016/j.jag.2022.103145).
- [45] K. Tan et al., "Discriminating forest leaf and wood components in TLS point clouds at single-scan level using derived geometric quantities," *IEEE Trans. Geosci. Remote Sens.*, vol. 60, 2022, Art. no. 5701517, doi: [10.1109/tgrs.2021.3121256](https://doi.org/10.1109/tgrs.2021.3121256).
- [46] J. Singh, S. R. Levick, M. Guderle, and C. Schmillius, "Moving from plot-based to hillslope-scale assessments of Savanna vegetation structure with long-range terrestrial laser scanning (LR-TLS)," *Int. J. Appl. Earth Observ. Geoinf.*, vol. 90, 2020, Art. no. 102070, doi: [10.1016/j.jag.2020.102070](https://doi.org/10.1016/j.jag.2020.102070).
- [47] C. Liu et al., "Context-aware network for semantic segmentation toward large-scale point clouds in urban environments," *IEEE Trans. Geosci. Remote Sens.*, vol. 60, 2022, Art. no. 5703915, doi: [10.1109/tgrs.2022.3182776](https://doi.org/10.1109/tgrs.2022.3182776).
- [48] C. Paris, D. Kelbe, J. van Aardt, and L. Bruzzone, "A novel automatic method for the fusion of ALS and TLS LiDAR data for robust assessment of tree crown structure," *IEEE Trans. Geosci. Remote Sens.*, vol. 55, no. 7, pp. 3679–3693, Jul. 2017, doi: [10.1109/tgrs.2017.2675963](https://doi.org/10.1109/tgrs.2017.2675963).



**Zekun Yang** received the B.S. degree in geographic information science in 2022 from the School of Earth and Space Sciences, Peking University, Beijing, China, where he is currently working toward the Ph.D. degree in cartography and geographic information system.

His research interests include vegetation remote sensing and remote sensing big data.



**Yanjun Su** received the B.E. degree in surveying and mapping engineering from China University of Geosciences, Beijing, China, in 2009, the M.S. degree in geographic information science from the Institute of Geographic Sciences and Natural Resources Research, Chinese Academy of Sciences, Beijing, China, in 2012, and the Ph.D. degree in environmental systems from the University of California at Merced, Merced, CA, USA, in 2017.

He is currently a Professor with the Institute of Botany, Chinese Academy of Sciences, Beijing, China. His research interests include applying geographic information science and remote sensing to understand the influence of anthropogenic activities and global climate change on terrestrial ecosystems, with a particular emphasis on the terrestrial carbon cycle, terrestrial biodiversity, energy balance, and land-use/land-cover change.



**Wenkai Li** received the B.S. degree in environmental science from Sun Yat-sen University, Guangzhou, China, in 2005, the M.S. degree in environmental engineering from Peking University, Beijing, China, in 2008, and the Ph.D. degree in environmental systems from the University of California, Merced, CA, USA, in 2013.

He is currently an Associate Professor with the School of Geography and Planning, Sun Yat-sen University, Guangzhou, China. His research interests include image classification, ecological niche modeling, radiative transfer modeling, and lidar remote sensing.



**Kai Cheng** received the B.E. degree in surveying and mapping engineering from the China University of Petroleum, Dongying, East China, in 2014, the M.S. degree in geodesy and survey engineering from China University of Mining and Technology, Beijing, China, in 2017, and the Ph.D. degree in geographic information system from the Institute of Geographic Sciences and Natural Resources Research, Chinese Academy of Sciences, Beijing, China, in 2020.

He is currently a Postdoctor with the School of Earth and Space Sciences, Peking University, Beijing, China. His research interests include applying remote sensing to describe spatial-temporal pattern of planted forest ecosystem and its ecological effects.



**Tianyu Hu** received the B.S. degree in ecology from the China Agriculture University, Beijing, China, in 2008, and the Ph.D. degree in ecology from the Institute of Botany, Chinese Academy of Sciences, Beijing, China, in 2014.

He is currently an Associate Professor with the Institute of Botany, Chinese Academy of Sciences, Beijing, China. His research interests include using LiDAR technology and dynamic vegetation model to understand forest ecosystem, especially in forest structure, function, and biodiversity.



**Hongcan Guan** received the B.S. degree in remote sensing science and technology from Wuhan University, Wuhan, China, in 2014, the M.S. degree in electronics and communication engineering from the Institute of Opto-electronics, Chinese Academy of Sciences, Beijing, China, in 2017, and the Ph.D. degree in ecology from the Institute of Botany, Chinese Academy of Sciences, in 2021.

He is currently an Associate Professor with the School of Tropical Agriculture and Forestry, Hainan University, Haikou, China. His research interests include using remote sensing technology to solve vegetation mapping-related challenges.



**Guangcai Xu** received the B.S. and M.S. degrees in geographic information science from Nanjing Forestry University, Nanjing, China, in 2004 and 2007, respectively, and the Ph.D. degree in forest management from the Chinese Academy of Forestry Sciences, Beijing, China, in 2011.

He is currently a Senior Engineer with Beijing GreenValley Technology Company, Ltd., Beijing, China. His research interests include using LiDAR technology to understand forest ecosystem and building extraction.



**Yu Ren** received the B.E. degree in remote sensing science and technology, in 2015, and the M.S. degree in geology, in 2018, both from the Chengdu University of Technology, Chengdu, China and the Ph.D. degree in cartography and geography information system from the Aerospace Information Research Institute, Chinese Academy of Sciences, Beijing, China, in 2021.

She is currently a Postdoctoral Researcher with School of Earth and Space Sciences, Peking University, Beijing, China. Her research interests include applying geographic information science and remote sensing to understand the terrestrial biodiversity, and some other ecology and agriculture problems.



**Qinghua Guo** received the B.S. degree in environmental science and the M.S. degree in remote sensing and geographic information system (GIS) from Peking University, Beijing, China, in 1996 and 1999, respectively, and the Ph.D. degree in environmental science from the University of California, Berkeley, CA, USA, in 2005.

He is currently a Professor with School of Earth and Space Sciences, Peking University, Beijing, China. He is also an Adjunct Professor and a member of the founding faculty with the School of Engineering, University of California at Merced, Merced, CA, USA. His research interests include GIS and remote sensing algorithm development and their environmental applications, such as object-based image analysis, geographic one-class data analysis, and LiDAR data.